

Misalignment of the Lense-Thirring precession by an accretion torque

D.A. Bollimpalli ^{1,2}, J. Horák ^{3,4}, W. Kluźniak ^{4,5}, and P. C. Fragile ⁶

¹ Department of Astronomy, Astrophysics & Space Engineering, Indian Institute of Technology Indore, Simrol, Indore 453552, Madhya Pradesh, India

e-mail: dbollimpalli@iiti.ac.in

² Center for Interdisciplinary Exploration & Research in Astrophysics (CIERA), Physics & Astronomy, Northwestern University, Evanston, IL 60202, USA

³ Astronomical Institute, Academy of Sciences, Boční II 141 31 Prague 4, Czech Republic

e-mail: horak@astro.cas.cz

⁴ Nicolaus Copernicus Astronomical Center, ul. Bartycka 18, PL 00-716 Warsaw, Poland

e-mail: wlodek@camk.edu.pl

⁵ Nicolaus Copernicus Superior School, College of Astronomy and Natural Sciences, ul. Gregorkiewicza 3, 87-100, Toruń, Poland

⁶ Department of Physics and Astronomy, College of Charleston, 66 George St, Charleston, SC 29424, USA

e-mail: fragilep@cofc.edu

Received September 15, 1996; accepted March 16, 1997

ABSTRACT

Context. Orbiting matter misaligned with a spinning black hole undergoes Lense-Thirring precession, due to the frame-dragging effect. This phenomenon is particularly relevant for type-C QPOs observed in the hard states of low-mass X-ray binaries. However, the accretion flow in these hard states is complex, consisting of a geometrically thick, hot corona surrounded by a geometrically thin, cold disk. Recent simulations have demonstrated that, in such a truncated disk scenario, the precession of the inner hot corona slows due to its interaction with the outer cold disk.

Aims. This paper aims to provide an analytical description of the precession of an inner (hot) torus in the presence of accretion torques exerted by the outer (cold) disk.

Methods. Using the angular momentum conservation equation, we investigate the evolution of the torus angular momentum vector for various models of accretion torque.

Results. We find that, in general, an accretion torque tilts the axis of precession away from the black hole spin axis. In all models, if the accretion torque is sufficiently strong, it can halt the precession; any perturbation from this stalled state will cause the torus to precess around an axis that is misaligned with the black hole spin axis.

Conclusions. The accretion torque exerted by the outer thin disk can cause precession around an axis that is neither aligned with the black hole spin axis nor perpendicular to the plane of the disk. This finding may have significant observational implications, as the jet direction, if aligned with the angular momentum axis of the torus, may no longer reliably indicate the black hole spin axis or the orientation of the outer accretion disk.

Key words. Accretion, accretion disks – Stars: black holes – X-rays: binaries – Relativistic processes – Hydrodynamics

1. Introduction

Quasi-periodic oscillations (QPOs) in the X-ray light curves of accreting black hole and neutron star X-ray binary systems, characterized by broad peaks in their power spectra, are a characteristic feature of these systems. The "quasi-periodic" nature arises from the modulation of either the frequency or the amplitude of the light curves. QPOs offer a unique opportunity to study the strong gravitational fields surrounding compact objects, providing insights into physical processes on spatial scales that are otherwise inaccessible, with the exception of nearby supermassive black holes observed by the Event Horizon Telescope. Based on their frequency, black hole QPOs are typically categorized as either high frequency (≥ 60 Hz) or low (≤ 30 Hz).

In addition to rapid variability, accreting black hole X-ray binaries exhibit spectral state transitions over periods ranging from days to months (e.g. Corral-Santana et al. 2016). These transitions, often depicted as q-shaped tracks in hardness-intensity

diagrams, reflect significant changes in the geometry and physical conditions of the accretion flow (Fender et al. 2004; McClintock & Remillard 2006). The primary spectral states are classified as "soft" and "hard," though intermediate states have also been observed. In the soft state, the X-ray spectrum is dominated by thermal emission, resembling blackbody radiation from a cool, optically thick, geometrically thin accretion disk. In contrast, the hard state is dominated by a non-thermal, power-law emission produced by Compton upscattering of soft seed photons from the disk by a hot, optically thin electron cloud, commonly referred to as the "corona."

While the precise geometry of the corona remains uncertain, a widely accepted model envisions a truncated disk, where the inner thin disk is replaced by a corona. As the system evolves from the hard to the soft state, the disk migrates inward, and the corona collapses, eventually reaching the innermost stable circular orbit.

QPOs are observed across different spectral states, with low-frequency QPOs (LFQPOs) being particularly prominent. Type-A and type-B LFQPOs typically appear during transitions through the intermediate states toward the soft state, while type-C LFQPOs appear mostly in the hard state. High-frequency QPOs, on the other hand, tend to occur in high-luminosity accretion states. Several models attribute QPOs to oscillations in the corona or the thin disk, or to waves generated by instabilities within the accretion flow¹. Understanding the origin and mechanisms driving QPOs may be helpful in constraining the geometry and location of the corona.

One of the most common interpretations of the type-C LFQPO is that it results from Lense-Thirring precession of the corona. This hypothesis is supported by observations showing that the QPO amplitude and phase lag between hard and soft photons, measured at the QPO frequency, depend strongly on the inclination angle of the system (Motta et al. 2015; van den Eijnden et al. 2017). In the truncated-disk model, the precession of the corona, surrounded by the truncated disk, produces the type-C LFQPOs (Ingram et al. 2009; Ingram & Done 2011). This model also explains the observed correlation between the low-frequency break (attributed to the viscous timescale at the transition radius) and the type-C QPO frequency (attributed to the precession frequency of the inner hot flow) in the power spectra of accreting black hole systems. The model has been further explored in great detail to include time-dependent emission of iron-line profiles arising from the variable orientation of the hot inner flow and the outer thin disk with respect to the observer (Ingram & Done 2012b; Ingram et al. 2016), correlation of the X-ray (Zycki et al. 2016) and optical (Veledina & Poutanen 2015) spectral properties with QPO phase, as well as variable X-ray polarization (Ingram et al. 2015).

Lense-Thirring Precession

A sufficiently hot, orbiting fluid around a Kerr black hole may take the shape of a torus. Among the eigenmodes of this torus (assuming it is slender) are rigid-body motions, the simplest being a uniform vertical² oscillation at a frequency corresponding to the vertical epicyclic frequency of a test particle, $\sigma = \omega_{\perp}$ (Bursa et al. 2004). This eigenmode is often invoked to explain high-frequency QPOs observed in X-ray binaries. This mode, characterized by identical vertical displacements of all fluid elements, corresponds to the $m = 0$ mode in a more general class of motions where vertical displacement varies azimuthally as $\exp(im\phi)$. The pattern frequency of these oscillations³ is given by $\omega_p = (\sigma + m\Omega)/m$, where Ω is the orbital frequency. The $m = -1$ mode, in particular, corresponds to a rigid-body precession of an inclined torus at a frequency defined by the difference between the orbital and vertical epicyclic frequencies:

$$\omega_p = \Omega - \omega_{\perp}. \quad (1)$$

This precession mechanism can be understood by considering the orbit of a test particle inclined at an angle to the equatorial plane of the black hole. Due to the frame-dragging effect of the spinning black hole, the orbit undergoes nodal precession,

¹ For a comprehensive review of QPOs and the suggested models, we refer the readers to Ingram & Motta (2019) and references therein.

² The vertical direction is taken to be along the spin axis of the black hole.

³ For a discussion of general modes (involving internal oscillations) of relativistic slender tori, see Blaes et al. (2006). We take the displacement to be proportional to $\exp[i(-\omega t + m\phi)]$.

known as Lense-Thirring precession (Lense & Thirring 1918). The vertical, epicyclic, rigid-body mode is thus thought to explain both the high and low-frequency QPOs (for $m = 0$ and $m = -1$, respectively) observed in X-ray binaries. (A similar combination of the *radial* epicyclic and orbital frequencies was suggested as an explanation for kHz QPOs in neutron stars by Stella & Vietri 1998; Stella et al. 1999).

A torus with a substantial radial extent can also undergo nearly rigid-body precession if the sound travel time across the torus is shorter than the precession period, $2\pi/\omega_p$. In this case, the Lense-Thirring torque is efficiently communicated through bending waves, causing the torus to behave as a solid body (Papaloizou & Terquem 1995; Lodato & Facchini 2013; Nixon & King 2016). The precession periods of non-slender tori have been derived analytically using perturbative expansions of the fluid equations (Blaes et al. 2007) (see also Straub & Šrámková 2009, for a full general relativistic treatment), and these precession frequencies match the form of equation (1), with radial averages replacing the orbital and vertical frequencies (Blaes et al. 2007).

Numerous general relativistic magnetohydrodynamic (GRMHD) simulations have confirmed the robustness of such nearly rigid-body Lense-Thirring precession of accreting tori (Fragile & Anninos 2005; Fragile et al. 2007; Morales Teixeira et al. 2014; Liska et al. 2018). In particular, Fragile et al. (2007) showed that the numerically derived precession rates agree well with the precession frequency for a rigid body (Liu & Melia 2002). Their derived expression for the precession frequency is a function of the inner and outer radii of the torus, based on the density and rotation profiles extracted from their simulations. These formulas have since been refined by Ingram et al. (2009); Ingram & Done (2011, 2012a) and De Falco & Motta (2018).

Note that in this case of free Lense-Thirring precession, the ‘tilt’ angle between the axes of the torus and the black hole remains constant over time. This means the angular momentum vector of the torus rotates uniformly about the black hole spin axis, sweeping out a conical surface.

However, in an astronomical context, the torus is typically the inner region of an accretion flow, surrounded by a disk. Notably, none of the studies listed above account for the effect of the outer disk on the torus precession. Only recently have GRMHD simulations of tilted, truncated accretion disks with inner tori demonstrated that the exchange of angular momentum between the outer thin disk and the torus introduces an accretion torque, which significantly alters the torus precession dynamics (Bollimpalli et al. 2023).

In this paper, we examine analytically the leading effects of an accretion torque on the Lense-Thirring precession of an inner torus within this theoretical context. We find that the torus precesses around an axis different from the black hole spin axis. In other words, the precession occurs around an axis that is neither aligned with the black hole spin axis, nor perpendicular to the plane of the accretion disk. This finding has important observational implications, particularly if the jet is aligned with the angular momentum axis of the torus. In such a scenario, the jet direction may no longer be reliably used to infer the black hole spin axis or the orientation of the outer accretion disk.

The rest of the paper is organized as follows: In § 2, we present the basic framework of our model, which is based on the truncated disk geometry. § 3 derives the general solution for the precession of a tilted, accreting torus. In § 4, we provide specific examples of different accretion torques and demonstrate how precession occurs in each case. § 5 compares our results with recent simulation findings from Bollimpalli et al. (2023). Finally,

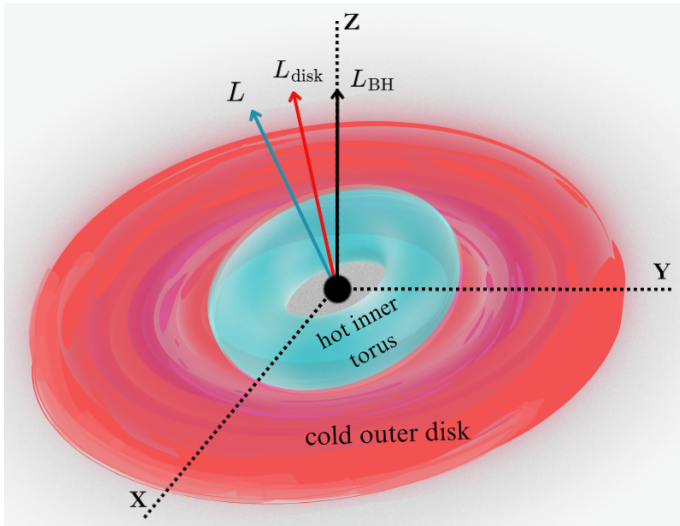


Fig. 1. Geometry of our model. The direction of the black-hole angular momentum \mathbf{L}_{BH} coincides with the z -direction of the Cartesian system used in the calculations. Due to misalignment with the black-hole spin, the angular momenta of the outer thin accretion disk (\mathbf{L}_{disk}) and inner hot torus (\mathbf{L}) have nonzero projections into the x - y plane.

in § 6, we discuss the observational implications and present our conclusions.

2. The overall picture

We imagine a spinning black hole with its axis misaligned with respect to the accretion flow. We consider the two-component accretion flow geometry that is thought to be relevant for hard states of low-mass X-ray binaries (LMXBs), i.e., an inner, hot torus surrounded by an outer cool, thin disk, as shown in Fig. 1. Since the inner torus is geometrically thick and optically thin, bending waves are communicated efficiently for the torus to precess as a rigid-body⁴. On the other hand, due to the geometrically thin and optically thick nature of the outer disk, the bending waves are diffused away and we expect no precession in this region.

The accretion flow is tilted in that if we align the z axis of a Cartesian coordinate frame with the spin axis of the black hole (the "vertical" direction, see Fig. 1), the angular momentum vector of the disk has a nonzero projection onto the x - y plane. Thus, any accretion from the disk onto the torus will tend to change the x - y component of the torus angular momentum through the advection of the disk angular momentum (in addition to affecting the z component). This will result in a rotation in the x - y plane of the projection of the angular momentum onto it, beyond any relativistic precession, if the torus is already tilted with respect to the black hole spin axis. Alternatively, it will tilt the torus if it happens to be aligned with the black hole. The net advection rate of the angular momentum into the torus is equivalent to a torque, which we call the accretion torque. Our aim is to derive the time evolution of the angular momentum of the torus for a given accretion torque, and in particular to discuss the direction in which the torus axis will point. More specifically, we are interested in the evolution of the precession angle of the torus, defined as the angle from the x axis to the x - y projection of the torus angular momentum vector.

⁴ If the inner torus were not accreting from the outer disk, it would be able to undergo free Lense-Thirring precession, as discussed in the introduction.

3. The torque equation

For our purposes, it is sufficient to use a Newtonian equation of angular momentum conservation,

$$\frac{d\mathbf{L}}{dt} = \boldsymbol{\tau}, \quad (2)$$

with $\boldsymbol{\tau} = \boldsymbol{\tau}_p + \boldsymbol{\tau}_{\text{acc}}$. We include the main effect of general relativity by adopting a Lense-Thirring torque

$$\boldsymbol{\tau}_p = \boldsymbol{\omega}_p \times \mathbf{L}, \quad (3)$$

where $\boldsymbol{\omega}_p = 2(G/c^2)(\mathbf{L}_{\text{BH}}/R^3)$ is a constant vector in the vertical (black hole spin) direction, \mathbf{L}_{BH} is the black-hole angular momentum, and R is a torus mean radius (Wilkins 1972; Bardeen & Petterson 1975). In effect, we assume that the torus has a constant free precession rate, $\boldsymbol{\omega}_p$, regardless of its mass and total angular momentum \mathbf{L} . The second component of the torque, $\boldsymbol{\tau}_{\text{acc}}$, is the accretion torque equal to the net rate of angular momentum advection. Thus, the evolution of the torus angular momentum is given by

$$\frac{d\mathbf{L}}{dt} = \boldsymbol{\omega}_p \times \mathbf{L} + \boldsymbol{\tau}_{\text{acc}}. \quad (4)$$

Note that we have ignored the viscous terms in the above conservation equation, as they were found to be negligible when compared to the Lense-Thirring torque and angular momentum fluxes in the simulations of Bollimpalli et al. (2023).

In the Cartesian coordinate system introduced in the previous Section, $\boldsymbol{\omega}_p = \omega_p \hat{z}$, and hence $\boldsymbol{\tau}_p$ does not depend on L_z . Therefore the z component of the torque equation

$$\frac{dL_z}{dt} = (\boldsymbol{\tau}_{\text{acc}})_z \quad (5)$$

does not couple to the x and y components, and it is the latter components that we focus on in our analysis. Introducing complex variables:

$$L \equiv L_x + iL_y, \quad (6)$$

so that $L_x = \text{Re } L$, $L_y = \text{Im } L$, and similarly for $\boldsymbol{\tau}_{\text{acc}}$, we can rewrite the x and y components of Eq. (4) as

$$\frac{dL}{dt} = i\omega_p L + \tau_{\text{acc}}. \quad (7)$$

For $\tau_{\text{acc}} = 0$ the equation has a simple solution corresponding to uniform rotation in the positive direction

$$L(t) = L_0 \exp(i\omega_p t) \equiv L_{\text{LT}}(t). \quad (8)$$

This is just the x - y projection of the angular momentum vector of the torus undergoing Lense-Thirring free precession, hence the notation.

Note that precession may be halted for a sufficiently large accretion torque (or sufficiently small tilt angle of the torus). It suffices that the following equation be satisfied, starting at some instant t_0 ,

$$\boldsymbol{\tau}_{\text{acc}} = -\boldsymbol{\omega}_p \times \mathbf{L}, \quad (9)$$

for $d\mathbf{L}/dt = 0$ to hold for $t > t_0$. In the x - y plane, this is just

$$\tau_{\text{acc}} = -i\omega_p L, \quad (10)$$

and has a simple interpretation. The Lense-Thirring torque being perpendicular to the angular momentum vector leads it in phase

by $\pi/2$ (factor of i), so an accretion torque of equal magnitude but in opposite direction will counteract it, also being perpendicular to the angular momentum vector, but lagging it by the same phase angle $\pi/2$ (factor of $-i$).

However, this equilibrium point, let us call it L_1 , corresponding to $\tau_{\text{acc}} = \tau_1$ is not stable: a small fluctuation of L will lead to resumption of precession (about the equilibrium point L_1). Indeed, keeping $\tau_1 = -i\omega_p L_1$ fixed, a change of L from L_1 to L_2 at time t_2 will lead to the resumption of precession for $t > t_2$ with $L_0 = L_2 - L_1$, by Eqs. 7, 8, 10. A similar result would be obtained upon an impulsive change of the accretion torque τ_{acc} from the value τ_1 to τ_2 , with the precession now occurring around the point of equilibrium $L_2 = i\tau_2/\omega_p$ with amplitude $L_0 = L_1 - L_2$. This is a generic result: a change of the accretion torque leads to a change in the precession, and in particular can induce a Lense-Thirring precession where there was none before, as will also be seen in our discussion in Subsection 4.3.

The general solution of the inhomogeneous linear differential Eq. (4) is the sum of the general solution of the homogeneous equation

$$\frac{dL}{dt} = i\omega_p L, \quad (11)$$

which we already know to be $L_{LT}(t)$, and a special solution of the inhomogeneous Eq. (4). Thus,

$$L(t) = L_{LT}(t) + \hat{L}(t), \quad (12)$$

where \hat{L} is a particular solution satisfying

$$\frac{d\hat{L}}{dt} = i\omega_p \hat{L} + \tau_{\text{acc}}. \quad (13)$$

To summarize, the general solution to the motion of a tilted, accreting torus is a precession (Eq. [8]) at the Lense-Thirring frequency around a (possibly moving) axis $\hat{L} \equiv \hat{L}_x + i\hat{L}_y$, given by the solution of Eq. (13), which can be taken as:

$$L(t) = \left(L_0 + \int \tau_{\text{acc}}(t') \exp(-i\omega_p t') dt' \right) \exp(i\omega_p t). \quad (14)$$

All that remains is to find $\hat{L}(t)$ and $L(t)$ for any given $\tau_{\text{acc}}(t)$, which is what we will address in the next section.

4. Solutions

We now give solutions of Eq. (13) for four simple forms of τ_{acc} . In steady state, it may be reasonable to assume that the net rate of angular momentum advection is constant in time. This corresponds to a steady torque (§ 4.1). On the other hand, the luminosity of X-ray binaries often varies in time. A steady rise in advected angular momentum rate (§ 4.2) may correspond to black hole disks going into ‘‘outburst.’’ A change of the accretion torque from one value to another (§ 4.3) could perhaps model state transitions of black hole binaries. Finally, it is possible that the ring of the accretion disk directly adjacent to the torus may itself precess, for instance in the corrugation mode of diskoseismology (Kato 1989; Silbergleit et al. 2001; Kato 1993; Ipser 1996). The x - y components of the advected angular momentum could then vary harmonically, so that the accretion torque could be taken to rotate at a definite frequency (§ 4.4).

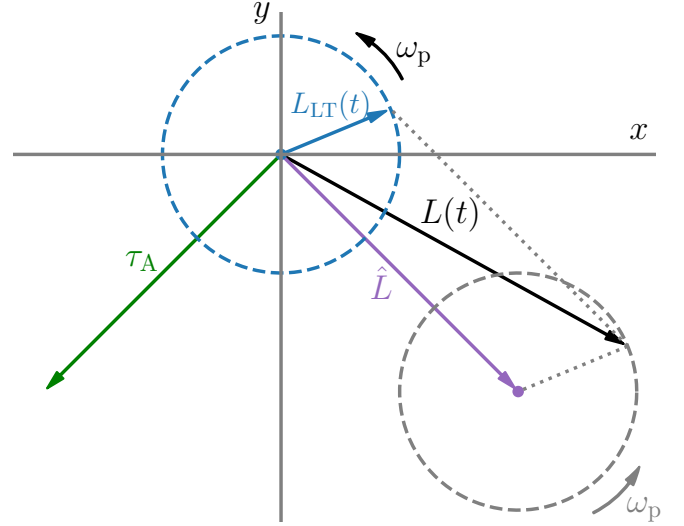


Fig. 2. Precession of the angular momentum vector L of the inner torus when a steady accretion torque $\tau_f = \tau_A$ is applied. This figure is projected into the plane perpendicular to the black-hole spin. In the absence of an accretion torque, the angular momentum vector executes free Lense-Thirring precession $L_{LT}(t)$ around the direction of the black hole spin. When the torque is applied, the general solution consists of free Lense-Thirring precession about a new direction (shifted by a constant, \hat{L}).

4.1. Steady accretion torque

For a steady torque, $\tau_{\text{acc}} = \tau_f = \text{const}$, the solution is

$$\hat{L} = \frac{i\tau_{\text{acc}}}{\omega_p} = \frac{i\tau_f}{\omega_p} = \text{const}. \quad (15)$$

The general solution of Eq. (7) is then

$$L(t) = \frac{i\tau_f}{\omega_p} + L_0 \exp(i\omega_p t), \quad (16)$$

describing a precession with the Lense-Thirring frequency about a point (in the x - y plane) which is advanced by $\pi/2$ in phase with respect to the accretion torque (see Fig. 2). The reason for this has already been given in the paragraph following Eq. (10). The amplitude of precession, L_0 , is given by the initial conditions.

4.2. Linearly growing torque

Taking $\tau_{\text{acc}}(t) = \tau_0 + (t/t_f)\tau_f$, we obtain

$$\hat{L}(t) = \frac{\tau_f}{t_f \omega_p^2} + \frac{i\tau_{\text{acc}}(t)}{\omega_p}. \quad (17)$$

In this case, the x - y projection of the tip of the angular momentum vector undergoes uniform circular motion at the Lense-Thirring precession rate, similar to the case in section 4.1. However, in this scenario, the point around which this precession occurs will experience linear drift in the direction that advances the accretion torque by $\pi/2$ in phase. In the limit of slow growth, $\omega_p t_f \gg 1$, this tends to the steady torque solution, albeit with a varying position of the center of precession, $\hat{L}(t) \approx i\tau_{\text{acc}}(t)/\omega_p$.

4.3. Change of torque

Let us consider a variation in torque that is exponentially changing from τ_1 to τ_f , with a decay constant ω_h ,

$$\tau_{\text{acc}}(t) = \tau_f + (\tau_1 - \tau_f) \exp(-\omega_h t). \quad (18)$$

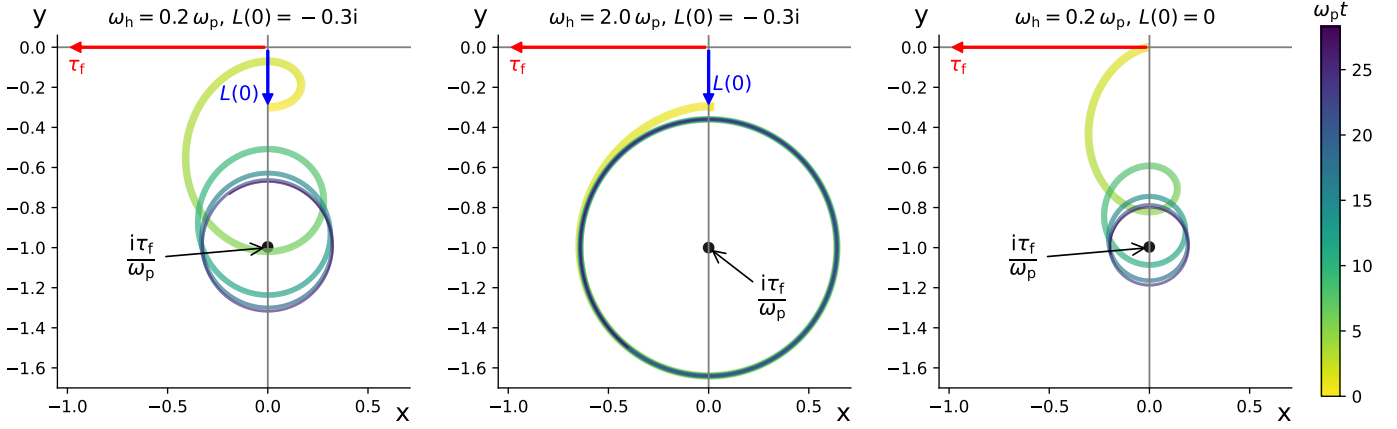


Fig. 3. Trajectory of the torus angular-momentum vector in the x - y plane when the accretion torque evolves exponentially from zero to $\tau_f = -1$ for various cases. A torus that is initially precessing with an angular momentum $L(0) = -0.3i$ approaches the final state of precession about the new equilibrium point, $i\tau_f/\omega_p$, slowly or rapidly for a low ($\omega_h = 0.2\omega_p$) or high ($\omega_h = 2\omega_p$) healing frequency, as shown in the *left* and *middle* panels, respectively. The *right* panel presents the same case as in the *left* (i.e., $\omega_h = 0.2\omega_p$), except that initially the torus has a zero angular momentum projection onto the x - y plane, i.e., $L(0) = 0$, highlighting our finding that the change in accretion torque can induce precession in a torus. In all three examples, we took $\omega_p = 1$ and the phase evolution is represented by both the colour and the decreasing thickness of the curve.

In this case, the particular solution takes the form

$$\hat{L}(t) = -\frac{\omega_h}{\omega_p^2 + \omega_h^2} (\tau_i - \tau_f) \exp(-\omega_h t) + i \left[\frac{\tau_f}{\omega_p} + \frac{\omega_p}{\omega_p^2 + \omega_h^2} (\tau_i - \tau_f) \exp(-\omega_h t) \right]. \quad (19)$$

This tends exponentially to the constant torque solution. When the change is slow, $\omega_h \ll \omega_p$, this approximates the steady torque solution, with a different value of the accretion torque at every instant of time: $\hat{L}(t) \approx i\tau_{\text{acc}}(t)/\omega_p$. In the opposite limit of fast healing, $\omega_p \ll \omega_h$, the solution is very close to the steady torque solution with the final value of the torque, $\hat{L}(t) \approx i\tau_f/\omega_p$.

A general solution consists of a free Lense-Thirring precession (8) and the special solution (19), whose properties were discussed above. Fig. 3 shows two such examples of how the torus angular momentum evolves for the fast ($\omega_h = 2\omega_p$; left panel) and slow ($\omega_h = 0.2\omega_p$; middle panel) change of the accretion torque from 0 to τ_f . Since the accretion torque is initially zero, the torus precesses around the z -axis. Interestingly, even if the initial torus is aligned with the black hole spin-axis, i.e., precession is zero, the accretion torque change can still excite free precession of the torus, as shown in the last panel of Fig 3.

One could similarly consider a change in torque that is oscillating between τ_A and τ_B at a frequency ω_h :

$$\tau_{\text{acc}}(t) = \frac{(\tau_A + \tau_B)}{2} + \frac{(\tau_B - \tau_A)}{2} \sin(\omega_h t), \quad (20)$$

for which the particular solution is given as

$$\hat{L}(t) = \frac{\omega_h}{\omega_p^2 - \omega_h^2} \frac{(\tau_B - \tau_A)}{2} \cos(\omega_h t) + i \left[\frac{(\tau_A + \tau_B)}{2\omega_p} + \frac{\omega_p}{\omega_p^2 - \omega_h^2} \frac{(\tau_B - \tau_A)}{2} \sin(\omega_h t) \right]. \quad (21)$$

4.4. Rotating torque

As a final case, we consider a rotating torque given by $\tau_{\text{acc}}(t) = \tau_f \exp(i\omega_1 t)$. We obtain the particular solution of the form

$$\hat{L}(t) = \frac{i\tau_f}{\omega_p - \omega_1} \exp(i\omega_1 t), \quad (22)$$

and the general solution, using Eqs. (12) and (8), reads

$$L(t) = L_0 \exp(i\omega_p t) + \frac{i\tau_f}{\omega_p - \omega_1} \exp(i\omega_1 t). \quad (23)$$

This solution passes through a resonance at $\omega_1 = \omega_p$. As $\omega_1 \rightarrow \omega_p$, the x - y component of the angular momentum vector L greatly increases in magnitude, implying that the torus tends to a position in which it “stands on its edge,” i.e., the plane of the torus approaches a vertical position (the torus axis becoming horizontal, i.e., tending to line up with the black-hole equatorial plane). An observer at infinity on the axis of the black hole would then see a constant aspect of the torus (no luminosity variation) as the torus precesses, while a distant observer in the equatorial plane of the black hole would presumably report large luminosity variations, seeing the torus edge-on every half precession period and face-on a quarter of a period later.

Perhaps the most interesting situation occurs when the two frequencies are close, but not exactly equal, and the amplitudes of both exponentials in Eq. 23 are comparable, i.e.: $\omega_1 \approx \omega_p$, but $\omega_1 \neq \omega_p$, and $|L_0| = |\tau_f|/(\omega_p - \omega_1)$. Then the general solution of Eq. (12), with Eqs. (8) and (22), would exhibit beats in which the amplitude of the x - y component of the angular momentum vector is modulated at the slow frequency $(\omega_p - \omega_1)/2$, while precessing at the fast frequency of $(\omega_1 + \omega_p)/2$. In this case, the modulation means that the midplane of the torus oscillates between a vertical position and the horizontal one, at the frequency of $(\omega_p - \omega_1)$. An example is shown in Fig. 4

5. Comparison with simulations

The Lense-Thirring precession of the inner torus is a widely accepted model for explaining type-C low-frequency QPOs typically observed in the hard or hard-intermediate states of LMXBs.

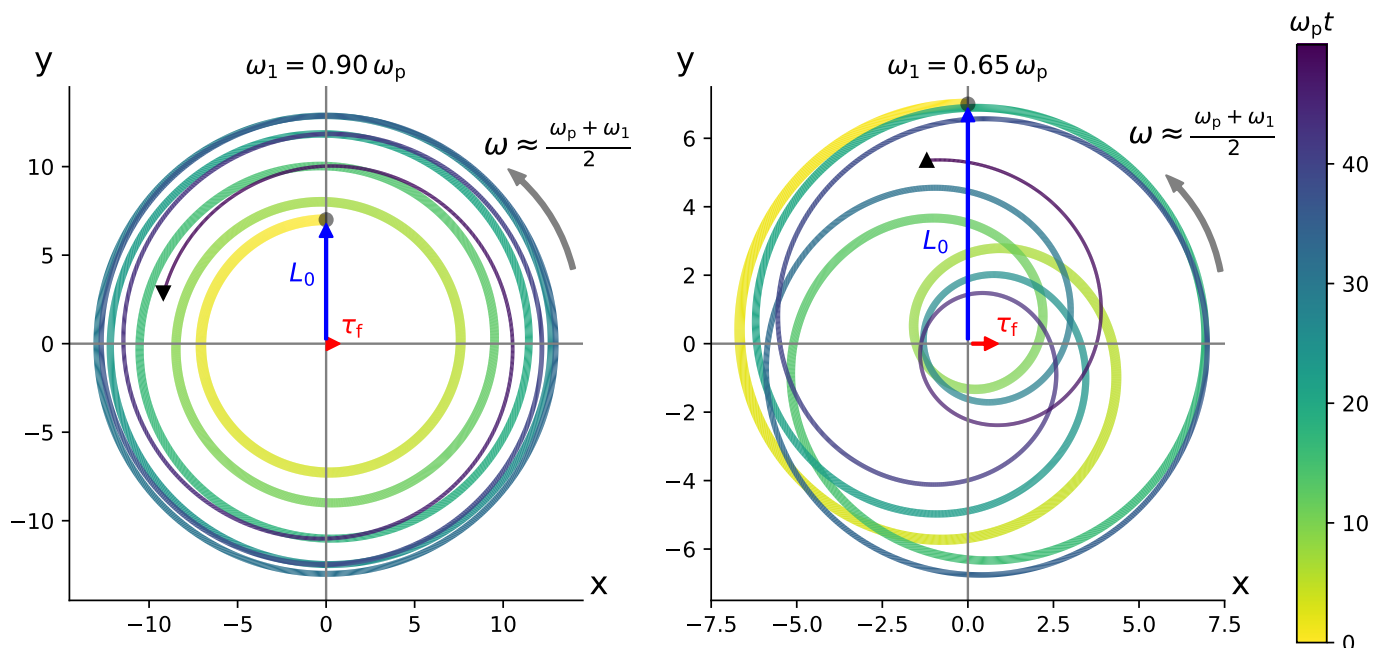


Fig. 4. Trajectory of the torus angular momentum vector in the x - y plane for an accretion torque rotating with frequency $\omega_1 = 0.9\omega_p$ (left panel) and $\omega_1 = 0.65\omega_p$ (right panel). In both cases, we use $L(0) = 7i$, $\tau_A = 1$, and $\omega_p = 1$. The phase of the trajectory is represented by both the color and the decreasing thickness of the curve, with the starting point at $t = 0$ and a point at some later time t marked by a circle and triangle, respectively (for visualization purposes). The torus precesses around the black hole axis with a frequency of $(\omega_p + \omega_1)/2$. Additionally, the tilt angle between the black hole and torus oscillates with frequency $(\omega_p - \omega_1)$.

Often, measurements of the type-C QPO frequency are used to constrain the torus size and the black hole parameters, disregarding the outer thin disk and assuming the torus precesses at the free Lense-Thirring frequency. However, simulations by Bollimpalli et al. (2023) have demonstrated that the outer thin disk can significantly impact the torus precession rate. Motivated by these findings, we analytically explored the effect of an accretion torque in this paper using simplified forms that mimic various astrophysical scenarios. We now validate our model using the data from simulation a9b15L4, originally detailed in Bollimpalli et al. (2023), which is extended to twice the duration initially reported in that paper. The initial setup of this simulation involves a torus extending up to $15 GM/c^2$ surrounded by a thin slab of gas, both initially misaligned with the black hole spin axis by 15 degrees. Further details of this simulation can be found in Bollimpalli et al. (2023, 2024).

For the initial phase of the simulation (up to $\sim 25000 GM/c^3$), as originally reported in Bollimpalli et al. (2023), the accretion torque and the Lense-Thirring torque are comparable in magnitude, as shown in the first panel of Fig. 5. Consequently, the precession rate of the torus decreases to only 5 percent of the expected free Lense-Thirring precession frequency (Bollimpalli et al. 2023). However, as the simulation proceeds, this balance is eventually disrupted, causing the torus to precess around a new axis. During this phase (i.e., $t \gtrsim 25000 GM/c^3$), the x and y components of the accretion torque exhibit oscillatory behavior, as shown by the solid curves in the second panel of Fig. 5. The oscillatory nature of the torque likely stems from the differential precession of the transition region between the outer thin disk and the torus as the simulation evolves. We employ the oscillating torque model described in section 4.3 to fit the accretion torque exerted on the torus region ($5 - 15 GM/c^2$). The best-fit results, obtained using Eq. 20, are shown in the second panel of Fig. 5. The best fit yielded a constant $\omega_h \approx 0.0005$,

while ω_p is taken to be the angular-momentum-weighted average of the Lense-Thirring precession frequency for a rigid body (see equation 15 of Ingram & Motta 2019):

$$\omega_p = \frac{\int_5^{15} \Omega_{LT} \Omega_\phi \Sigma(r) r^3 dr}{\int_5^{15} \Omega_\phi \Sigma(r) r^3 dr} \quad (24)$$

where $\Omega_{LT} = \sqrt{GM/r^3} \left[1 - \sqrt{1 - 4a_*/r^{3/2} + 3a_*^2/r^2} \right]$ is the Lense-Thirring precession frequency of a test particle, and $a_* = 0.9$ and M are the dimensionless spin and mass of the black hole, respectively. We directly infer the radial profile of the time-averaged surface density, Σ , from the simulation. Subsequently, we utilize the best-fit values for τ_A and τ_B from Eq. 21 to compute the x and y components of the total angular momentum L , which are shown in the third panel of Fig. 5.

This exercise underscores the significant influence of the outer thin disk on both the precession rate and the axis of precession. It appears that the initially reported phase of precession in Bollimpalli et al. (2023) was transient. The later oscillatory behavior highlighted in this section could also be transient; bending waves excited in the inner region propagate outward, inducing precession in the outer thin disk for a brief period before dissipating as they diffuse away. However, since the angular momentum from this region will eventually reach the inner regions, it impacts the precession. To comprehend these intricate dynamics better, our future plan involves running these simulations for a longer period.

6. Discussion and conclusions

The two-component model, where an inner hot, geometrically thick accretion flow forms a torus-like structure and is surrounded

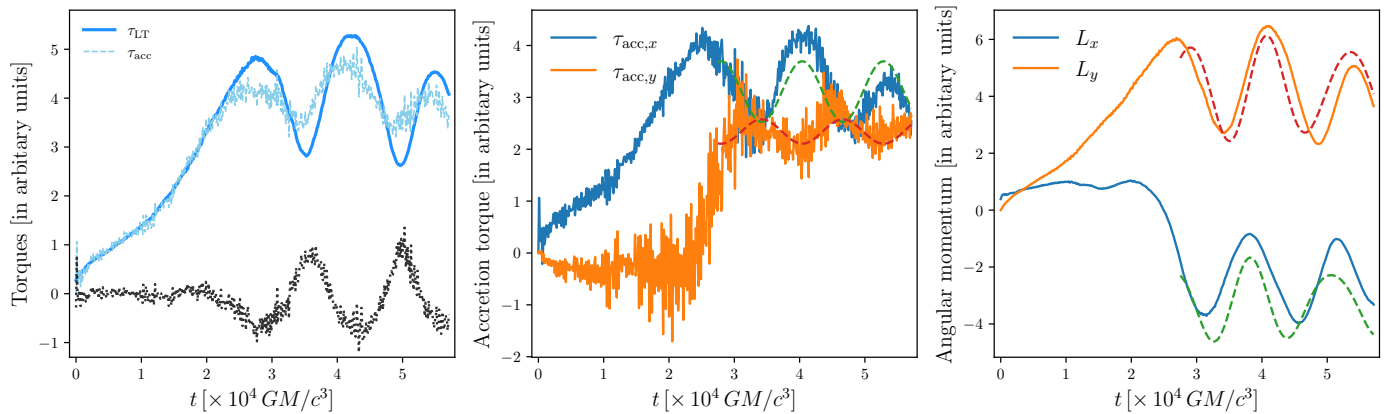


Fig. 5. Comparison of our model with the simulation data of Bollimpalli et al. (2024). In the *left* panel, we show the magnitude of the accretion (dashed curve) and Lense-Thirring (solid curve) torques integrated over the torus region, i.e. $5 - 15 GM/c^2$. The residual between the two (black, dotted curve) remains close to zero in the initial phase of the simulation, up to $\sim 25000 GM/c^3$. The *middle* panel shows the x and y components of the net accretion torque on the torus (solid curves), and their respective fits using Eq. 20 (dashed curves). Finally, the *right* panel shows the the x and y components of the total angular momentum of the torus (solid curves), and their respective fits using Eq. 21 (dashed curves).

by a cold standard accretion disk, is a popular framework for explaining a rich phenomenology of observational properties of accreting black holes in low-mass X-ray binaries. For instance, the photon spectrum may be fitted by a thin accretion disk truncated at some radius and a hotter component identified with the inner torus. When it comes to the observed X-ray variability, the highest frequency QPOs may be explained by the $m = 0$ vertical epicyclic mode of the torus (Bursa et al. 2004), while the type-C QPO may be identified with the $m = -1$ vertical epicyclic mode (Fragile et al. 2007; Blaes et al. 2006). Indeed, as demonstrated by numerous numerical simulations, the free torus responds to the Lense-Thirring torque exerted by a black hole by precessing as a rigid body, as long as the sound crossing time remains small compared to the precession period (Fragile et al. 2007; Liska et al. 2018). However, in reality the two components interact, so that free precession does not correctly describe the motion of the torus.

In a recent simulation where a torus was placed at the center of a truncated disk, its precession acquired a seemingly complicated character. When considered to be moving about the black hole axis, the torus started precessing at the Lense-Thirring frequency, but subsequently slowed down its precession and eventually seemed to stall, the axis of symmetry of the torus executing small loops about the position at which it stalled. We believe this behavior can be understood with the simple rigid-body mechanical model given in Eq. 4, when the angular momentum accreted with the matter from the outer cold disk is taken into account. This additional angular momentum flux corresponds to a new source term (an accretion torque) in the angular momentum conservation equation. In this paper, we have examined the precession of the inner torus in a few of the most natural situations corresponding to different prescribed accretion torques. The solutions, presented above, can be described as a precession around an axis which itself executes a definite motion. While, in general, the precession rate of the torus is itself quite robust and remains unaffected by the accretion torque, the accretion torque has a huge impact on the precession amplitude, as well as on the precession axis, or the mean orientation (tilt angle time averaged over the precession period) of the torus.

Already the simplest case of a constant (steady) accretion torque described in Sec. 4.1 brings interesting results. In that case, the inner torus still precesses with the same rate as given

by the Lense-Thirring frequency, however, the mean direction of the angular momentum vector corresponds neither to the black-hole spin, nor to the orientation of the outer disk. Instead, it results from the balance between the Lense-Thirring torque τ_p and the accretion torque τ_f applied by the outer disk, and the angle the mean direction of the torus axis makes with the black-hole spin is $\beta(t) = \arctan[|\hat{L}|/L_z(t)]$, where \hat{L} is the (constant) projection onto the x - y plane of the angular momentum vector, as determined by the accretion torque, c.f. Eq. 15.

These findings have important implications for models of correlations of the spectral properties of black hole LMXBs with the phase of type-C QPOs. Although the precession rate of the inner flow is still the same, its radiation illuminates different parts of the outer accretion disk differently than expected, leading to different reflection spectra (Ingram & Done 2012b; Ingram et al. 2016) and polarization (Ingram et al. 2015).

We also considered (in Sec. 4.2 and 4.3) two situations in which the accretion torque changes gradually in time. In both cases, a slow “adiabatic” change of torque just leads to a sequence of steady precession states, i.e., on top of a free Lense-Thirring precession that remains unaffected, the mean direction of the torus angular momentum gradually changes according to the instant accretion torque. An interesting effect occurs when the rate of torque change becomes comparable to the magnitude of the precession period or larger, i.e. when $(d\tau_{acc}/dt) \geq O(\omega_p)\tau_{acc}$. The inner torus responds to these changes by increasing or decreasing the precession amplitude (depending on the relative orientation of the torus angular momentum and the torque change), in addition to the gradual change of the torus mean tilt angle (see Fig. 3). As noted already, state transitions in black hole LMXBs are likely accompanied by changes in the overall geometry of the accretion flow, and it is therefore natural to assume that the torque exerted by the outer accretion disk on the inner torus will change. Our results show that these changes may even occasionally amplify the Lense-Thirring precession of the inner flow.

Finally, we have studied situations in which the accretion torque changes periodically in time (Sec. 4.4). This may happen when the surrounding parts of the outer disk undergo periodic changes either due to the presence of trapped, low-frequency oscillation modes (e.g. the corrugation mode), or when the accretion rate is modulated periodically. In that case, the torque equation takes the form of a forced linear oscillator. The res-

onance, occurring when the frequency of the accretion torque matches the precession rate of the inner torus, strongly enhances the inclination of the torus with respect to the black-hole spin. Near the resonance, the torus undergoes low-frequency changes of its inclination, in addition to its precession.

Acknowledgements. Part of this work was supported by the German *Deutsche Forschungsgemeinschaft*, DFG project number Ts 17/2–1. Research supported in part by the Polish NCN grant No. 2019/33/B/ST9/01564. PCF gratefully acknowledges the support of NASA through award No 23-ATP23-0100. DAB acknowledges support from IIT-Indore, through a Young Faculty Research Seed Grant (project: ‘INSIGHT’; IITI/YFRSG/2024-25/Phase-VII/02). JH acknowledges support of the the Czech Science Foundation (GAČR) grant No. 21-06825X.

References

- Bardeen, J. M. & Petterson, J. A. 1975, *ApJ*, 195, L65
- Blaes, O. M., Arras, P., & Fragile, P. C. 2006, *MNRAS*, 369, 1235
- Blaes, O. M., Šrámková, E., Abramowicz, M. A., Kluźniak, W., & Torkelsson, U. 2007, *ApJ*, 665, 642
- Bollimpalli, D. A., Fragile, P. C., Dewberry, J. W., & Kluźniak, W. 2024, *MNRAS*, 528, 1142
- Bollimpalli, D. A., Fragile, P. C., & Kluźniak, W. 2023, *MNRAS*, 520, L79
- Bursa, M., Abramowicz, M. A., Karas, V., & Kluźniak, W. 2004, *ApJ*, 617, L45
- Corral-Santana, J. M., Casares, J., Muñoz-Darias, T., et al. 2016, *A&A*, 587, A61
- De Falco, V. & Motta, S. 2018, *MNRAS*, 476, 2040
- Fender, R. P., Belloni, T. M., & Gallo, E. 2004, *MNRAS*, 355, 1105
- Fragile, P. C. & Anninos, P. 2005, *ApJ*, 623, 347
- Fragile, P. C., Blaes, O. M., Anninos, P., & Salmonson, J. D. 2007, *ApJ*, 668, 417
- Ingram, A. & Done, C. 2011, *MNRAS*, 415, 2323
- Ingram, A. & Done, C. 2012a, *MNRAS*, 419, 2369
- Ingram, A. & Done, C. 2012b, *MNRAS*, 427, 934
- Ingram, A., Done, C., & Fragile, P. C. 2009, *MNRAS*, 397, L101
- Ingram, A., Maccarone, T. J., Poutanen, J., & Krawczynski, H. 2015, *ApJ*, 807, 53
- Ingram, A., van der Klis, M., Middleton, M., et al. 2016, *MNRAS*, 461, 1967
- Ingram, A. R. & Motta, S. E. 2019, *New A Rev.*, 85, 101524
- Ipser, J. R. 1996, *ApJ*, 458, 508
- Kato, S. 1989, *PASJ*, 41, 745
- Kato, S. 1993, *PASJ*, 45, 219
- Lense, J. & Thirring, H. 1918, *Physikalische Zeitschrift*, 19, 156
- Liska, M., Hesp, C., Tchekhovskoy, A., et al. 2018, *MNRAS*, 474, L81
- Liu, S. & Melia, F. 2002, *ApJ*, 573, L23
- Lodato, G. & Facchini, S. 2013, *MNRAS*, 433, 2157
- McClintock, J. E. & Remillard, R. A. 2006, in *Compact stellar X-ray sources*, Vol. 39, 157–213
- Morales Teixeira, D., Fragile, P. C., Zhuravlev, V. V., & Ivanov, P. B. 2014, *ApJ*, 796, 103
- Motta, S. E., Casella, P., Henze, M., et al. 2015, *MNRAS*, 447, 2059
- Nixon, C. & King, A. 2016, in *Lecture Notes in Physics*, ed. F. Haardt, V. Gorini, U. Moschella, A. Treves, & M. Colpi, Vol. 905 (Berlin Springer Verlag), 45
- Papaloizou, J. C. B. & Terquem, C. 1995, *MNRAS*, 274, 987
- Silbergleit, A. S., Wagoner, R. V., & Ortega-Rodríguez, M. 2001, *ApJ*, 548, 335
- Stella, L. & Vietri, M. 1998, *ApJ*, 492, L59
- Stella, L., Vietri, M., & Morsink, S. M. 1999, *ApJ*, 524, L63
- Straub, O. & Šrámková, E. 2009, *Classical and Quantum Gravity*, 26, 055011
- van den Eijnden, J., Ingram, A., Uttley, P., et al. 2017, *MNRAS*, 464, 2643
- Veledina, A. & Poutanen, J. 2015, *MNRAS*, 448, 939
- Wilkins, D. C. 1972, *Phys. Rev. D*, 5, 814
- Zycki, P. T., Done, C., & Ingram, A. 2016, arXiv e-prints, arXiv:1610.07871